LA-UR- 96- 2575

CONF-960767--44

Title: Comparison of Attenuation Correction Methods for TGS and SGS: Do We Really Need Selenium-75?

RECEIVED
AUG 26 1996
OSTI

Author(s): R. J. Estep
T. H Prettyman
G. A. Sheppard

Submitted to:
Institute of Nuclear Materials Management (INMM)
Annual Meeting
July 28 - August 1, 1996
Naples, Florida

MASTER

Los Alamos
NATIONAL LABORATORY

Form No. 836 R5
ST 2629 10/91

DISTRIBUTION OF THIS DOCUMENT IS UNLIMITED

DISCLAIMER

Portions of this document may be illegible in electronic image products. Images are produced from the best available original document.

DISCLAIMER

COMPARISON OF ATTENUATION CORRECTION METHODS FOR TGS AND SGS: DO WE REALLY NEED SELENIUM-75?

R. J. Estep, T. H. Prettyman, and G. A. Sheppard
Los Alamos National Laboratory
Los Alamos, New Mexico USA

ABSTRACT

We compared attenuation-coefficient mapping techniques for use in tomographic gamma scanner (TGS) image reconstructions to determine whether there is a significant improvement when using fully coupled methods. For the constrained least-squares image reconstruction method tested here, we found no significant improvement. We also compared the effectiveness of different transmission source combinations for 129- and 414-keV ^{239}Pu TGS assays. We concluded that the best source combination for TGS assays of ^{239}Pu and other isotopes is a mixture of ^{133}Ba, ^{54}Mn, and ^{60}Co. Three other source combinations were found to be at least as effective as ^{75}Se.

INTRODUCTION

The tomographic gamma scanner (TGS) method[1,2] for assaying transuranic waste in 208-1 drums has significantly increased the density range of drums that can be assayed accurately for ^{239}Pu using gamma-ray spectroscopy. Currently, the upper density limit on assays is imposed by count rate limitations of high-purity germanium (HPGe) spectroscopy systems; a ^{75}Se source that is intense enough to penetrate the center of a dense drum with good counting statistics can be too intense to count when unattenuated. In this presentation we will examine four different attenuation mapping methods to see which gives the best results with higher density drums and noisy transmission data. In addition, we will examine alternatives to the usual transmission sources recommended for segmented gamma scanner[3] (SGS) assays to see if there are sources or combinations of sources more suitable for use in TGS assays of higher-density drums.

The strategy for SGS assays has been to select transmission sources with gamma-ray peaks that are close in energy to those in the radionuclide to be assayed. Thus, ^{75}Se has been the preferred transmission source for the assay of ^{239}Pu because its 121-, 136-, 280-, and 401-keV gamma rays are close in energy to the 129-, 203-, 375-, and 414-keV gamma-rays in ^{239}Pu. When the energies are this close, the emission gamma-ray attenuations can be estimated from the transmission data by a logarithmic interpolation or extrapolation. ^{75}Se is not a convenient source to use, however, as its 120-day halflife necessitates frequent replacement. Another drawback of this philosophy of source selection is that it recommends different transmission sources for the assay of different radionuclides.

TABLE I. SGS source combinations*

Isotope Assayed	Transmission Source
^{238}Pu 766.4 keV	^{137}Cs 661.6
^{239}Pu 413.7 keV	^{75}Se 400.1
^{235}U 185.7 keV	^{169}Yb 177.2,198.0 keV
^{238}U 1000.1 keV	^{54}Mn 834.8 keV
^{237}Np 311.9 keV	^{203}Hg 279.2 keV

*reprinted from Ref. 4

Table I lists the transmission source combinations recommended for the SGS assay of six isotopes. Using the table recommendations, for an SGS or TGS system to be capable of assaying all six isotopes requires a source wheel or ladder with six different transmission sources. Even if the source combinations examined here prove no more effective than ^{75}Se for assays of ^{239}Pu, there is some interest in finding combinations that are longer-lived or that can be used for multiple-isotope assays.

An idea that has emerged recently is to add a supplementary source with high energy lines to the usual transmission source to bolster poor data from the lower energy lines. Martz, et al.,[4] selected the long-lived, multi-energy [166m]Ho as a transmission source for use in their tomographic assay research. More recently, this approach has also been used with some success in the Los Alamos Waste Management Group's (LAWMG) mobile TGS system, which now routinely uses a ^{60}Co source in combination with ^{75}Se on dense-drum assays of [239]Pu.

Whatever the composition of the attenuating matrix, optimal use of the transmission data requires fitting the attenuation-coefficient as a function of energy. As the first step in a sophisticated analysis that produces accurate assays in 208-1 drums of up to 1 g/cm^3, the computer program TGS_ARC[5] implements what we will call here the data-coupled Z-effective method for mapping attenuation coefficients from transmission to emission energies. For each tomographic view the bulk effective atomic number (Z_{eff}) and atom density (n) are fitted to an approximation function for the attenuation coefficient (μ), which is then used to estimate what the transmissions would have been at the emission energies. In essence, one creates a set of surrogate data vectors for the emission energies and then reconstructs attenuation coefficient images from those. While this approach has worked well, improved fits should in principle be realized by coupling the energy and spatial dependence and simultaneously reconstructing attenuation-coefficient images for all energies at once. This can be done using either a fully coupled Z-effective method or the recently described material basis set (MBS) method.[6] Both are examined here.

BACKGROUND

The TGS transmission imaging problem can be written as[7]

$$v_{e,i} = \sum_j T_{ij} \mu_{e,j} \quad , \quad (1)$$

where

$e = 0,...,n_e-1$,
$i = 0,...,n_{views} - 1$, and
$j = 0,...,n_{voxels} - 1$.

The data vector element $v_{e,i}$ is the negative log of the transmission of the e'th transmission gamma

ray (of energy E_e) in the i'th tomographic view, $\mu_{e,j}$ is the attenuation coefficient in 1/cm of the j'th image voxel for the same energy, and the matrix element T_{ij} is the linear thickness of the j'th voxel along a ray connecting the transmission source and detector in the i'th view. There are n_e transmission gamma-ray energies, n_{views} tomographic views, and n_{voxels} volume elements in the reconstructed transmission image.

In the MBS method with n_z basis materials we write the attenuation coefficient for the j'th voxel at the e'th transmission energy as

$$\mu_{e,j} = \sum_z \rho_{z,j} U_{ez} \quad , \quad (2)$$

where

$$z = 0,...,n_z-1 \ .$$

The matrix element U_{ez} is the known attenuation coefficient in cm^2/g of the z'th basis material at the e'th energy and $\rho_{z,j}$ is the partial density in g/cm^3 of the z'th basis material in the j'th image voxel. After solving Eq.(2) for the partial density image vectors ρ_z, one can compute attenuation-coefficient image vectors $\mu_{e'}$ for any the set of emission energies (indexed by e') by constructing the matrix U' for the same material set at the new energies and computing

$$\mu_{e',j} = \sum_z \rho_{z,j} U'_{e'z} .$$

The transmission imaging problem can be coupled for all transmission energies and solved as a single large system of equations. To create the fully coupled system in the MBS method we substitute Eq.(2) for $\mu_{e,j}$ into Eq.(1) ,

$$v_{e,i} = \sum_j T_{ij} \sum_z \rho_{z,j} U_{ez} .$$

This can be rewritten as the linear system of equations

$$v_{i'} = \sum_{j'} R_{i'j'} \rho_{j'} \quad (3)$$

where

$R_{i'j'} = T_{ij} U_{ez}$,
$i' = e \cdot n_{views} + i$, and
$j' = z \cdot n_{voxels} + j$.

The vector **v** is now a combined logarithmic transmission vector of length $M = n_{views} \cdot n_e$ that spans all measurements at all energies, and the solution vector ρ is a combined density vector of

size $N = n_{voxels} \cdot n_z$ that spans all image voxels and every material in the MBS.

Alternatively, one can treat the energy and spatial components as being partially coupled in data space. To do this we define a set of n_{views} n_z-dimensional aggregate partial density vectors, ρ^*_i, as solutions to the n_{views} independent linear systems

$$v_{e,i} = \sum_z U_{ez} \rho^*_{i,z} .$$

At every view i we treat the $v_{e,i}$ as components of an n_e-dimensional vector and solve for ρ^*_i for that view. The aggregate density vectors can then be rearranged into n_z different n_{views}-dimensional vectors,

$$\{\rho^*_{i,z}\} \Rightarrow \{\rho^*_{z,i}\} ,$$

that become surrogate data vectors for solving the image reconstruction problem in the MBS representation. That is, we solve for the n_z partial density image vectors ρ_z using the original thickness matrix T of Eq.(1),

$$\rho^*_{z,i} = \sum_j T_{ij} \rho_{z,j} .$$

In the Z-effective model one treats all materials as if they were pure elements, which in some sense is complementary to the strict MBS model with $n_z = 2$. The maximum difference between the two models is about 7%, attained when comparing a mixture of equal masses of H and Pu (Z = 1 and 94) to the pure element La (Z = 57). In most realistic matrices the difference will be less than 4%. This difference is not significant for TGS assays, as a noticeable assay bias will only occur when the attenuation is severe, in which case statistical error will be more of a concern. In the Z-effective method we rewrite Eq. 2 as the non-linear function

$$\mu_{e,j} = f(E_e, Z_{eff,j}, n_j) ,$$

which can be substituted in the equations above to arrive at the Z-effective fully coupled and data-space coupled systems.

METHOD

COMPUTER SIMULATIONS To evaluate the relative merits of the attenuation-mapping schemes outlined above and to evaluate different transmission source combinations, we performed Monte Carlo simulations of single-layer TGS scans on a set of test cases. The simulations were created and fitted using the computer program TGS_FIT (version 3.0),[7] which has been extensively revised since its original release in January 1993.[8] TGS_FIT 3.0 supports multi-energy fitting of TGS and SGS scan data using either the MBS or Z-effective methods in both the data-space and full coupling schemes. The new version has a μ-calculator that uses bicubic interpolation on a table of known attenuation coefficients to estimate μ as a function of energy and atomic number. This general μ-calculator is used to generate arbitrary material basis sets, and also to create a set of cubic spline tables in equal Z-increments for fast computation of $\mu(Z, E_e)$ at just the transmission peak energies. This fast μ-calculator, which is used for fitting Z-effective, computes μ in roughly the time it takes to compute a cubic polynomial.

We simulated data by creating "true" density and radioactivity images and then generating the corresponding true data sets by direct matrix multiplication (e.g., as in Eq.(3)). The true data sets (net and background count rates) were then randomized to simulate realistic Poisson-distributed gamma-ray spectroscopy peak and background data. Thirty trials were run on each case so that the average behavior at the selected error level could be evaluated. All simulations were done on an IBM Thinkpad 760EL laptop computer running Microsoft Windows 95.

Simulation of the continuum background in the HPGe spectrum is important for evaluating transmission-source combinations, as a high-energy source such as ^{60}Co can increase the background level in the lower-energy spectrum. We estimated continuum background levels from experimental levels observed for ^{75}Se and ^{60}Co spectra taken with a 100% HPGe detector and interpolated the background levels to other energies for simulation of other source combinations. The observed background levels were approximately 5-12% of the main peak intensities in the ^{75}Se spectrum. When a ^{60}Co source was added to the ^{75}Se source, the background level for the 121-keV peak in ^{75}Se increased from 9% to 12%. We attempted to simulate this added background from high-energy peaks when simulating mixtures of different sources.

True attenuation-coefficient images can be specified in TGS_FIT either as attenuation coefficients, as mass density vectors in an MBS representation, or as (Z_{eff}, n) image pairs. For this study we used a three-element basis composed of C $(Z = 6)$, Cd $(Z = 48)$, and Pb $(Z = 82)$, and simulated matrices composed of just those materials.

TGS IMAGE RECONSTRUCTIONS TGS_FIT offers a choice of image reconstruction algorithms for multi-energy fitting that includes the non-negative least squares (NNLS) algorithm, the algebraic reconstruction technique, the expectation maximization algorithm, a maximum entropy algorithm, and a specialized nonlinear least squares algorithm that we are calling the sliding basis set (SBS) method for fitting Z-effective. For this study we have restricted ourselves to using the NNLS algorithm for all linear reconstructions and the SBS algorithm – which itself utilizes the NNLS algorithm – for fitting Z-effective. The NNLS algorithm is an active set method that repetitively uses singular value decomposition to solve unconstrained linear least squares problems as it searches model space for the optimal constrained solution. It is a decidedly poor algorithm for transmission imaging in TGS assays, and gives especially poor results in the uniform matrices studied here compared to the sophisticated methods used in, for example, the TGS_ARC code. The main reason for using it here is that it produces a graininess in the images that is highly correlated with the noise level in the data - a property that makes it undesirable for actual assays but useful for this comparison study.

Solving the nonlinear Z-effective problem in data space is fairly easy, but solving the fully coupled problem is tedious and slow using standard techniques. Fortunately, we can make use of the fact that (1) a two-element MBS solution (using, for example, C and Pb) will normally be within a few percent of the Z-effective solution; (2) a one-to-one relationship can be defined between a two-element MBS image and its corresponding Z-effective image; and (3) in the fully coupled scheme we can use a separate, independent material basis set for every image voxel. In the fully coupled SBS technique we make an initial fully coupled two-element

TABLE II. Relative gamma-ray strengths

Source	E_p (keV)	f_p	$f_p \cdot \varepsilon(E_p)$
75Se	121.1*	.0907	.091
	135.9	.3259	.302
	264.6**	.3398	.305
	279.5	.1431	.143
	400.7	.0612	.061
133Ba	302.9	.1357	.118
	356.0	.4647	.354
	383.9*	.0678	.049
60Co	1173.2	.5	.169
	1332.5	.5	.156
137Cs	661.6**	1	.501
54Mn	834.8	.8	.341
152Eu	121.8*	.2101	.21
	244.7*	.0552	.051
	344.3*	.1967	.153
	778.9	.0955	.043
	1085.9	.0717	.0256
	1112.1	.1001	.035
	1408.0	.1542	.046
166mHo	184.4	.2299	.232
	280.5	.0936	.081
	410.9**	.0364	.025
	711.7	.1843	.087
	752.3*	.0411	.019
	810.3	.1969	.086
	830.6	.0332	.014

* weak, **significant interference in Pu assays

MBS fit and then convert the partial density pairs $(\rho_{0,j}, \rho_{1,j})$ for each image voxel to a $(Z_{eff,j}, n_j)$ pair. We then replace the initial basis set at each image voxel with a custom two-element basis set that spans a smaller Z range and is centered (if possible) around $Z_{eff,j}$ for that voxel.

We then repeat the MBS fit to obtain a slightly better estimate of the Z-effective solution. This cycle is repeated 10 to 20 times using progressively narrower basis sets, so that the independent basis set at each voxel adiabatically closes on the Z-effective solution. Note that if a least squares method is used to solve the MBS part of the problem, then the SBS method will give the nonlinear least squares Z-effective solution. A simpler version of the SBS method is used in TGS_FIT to solve for Z-effective in data space.

SAMPLES The sample type chosen for study was a 6 by 6 resolution (10.2-cm voxels) single-layer uniform matrix with an idealized point

166mHo, 1200 y

137Cs, 30 y

152Eu, 13.6 y

133Ba, 10.5 y

60Co, 5.27 y

54Mn, 313 d

57Co, 271 d

75Se, 120 d

203Hg, 46.6 d

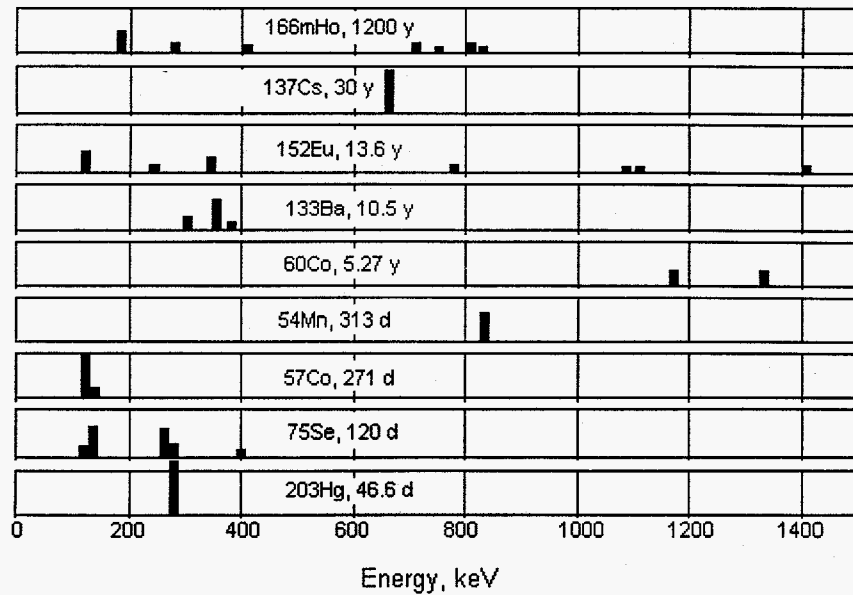0   200   400   600   800   1000   1200   1400

Energy, keV

Figure 1. The energies and relative unattenuated intensities of gamma rays in several radioactive sources. The intensities are scaled by typical counting efficiencies and represent equal count rate loads for each source.

emission source located slightly off from center. We modeled samples of this type with varying matrix density and elemental composition. The reconstructed mass of the idealized emission source (no noise was added to emission data) has been used as the figure-of-merit for evaluating goodness-of-fit for the transmission images. What makes this an attractive approach for evaluating attenuation mapping techniques and transmission source effectiveness is that when imaging this type of sample using the NNLS algorithm, the average error in the estimated mass tends to increase uniformly as the noise level in the transmission data increases. Assays with complex heterogeneous matrices, in contrast, may show a sudden loss of accuracy after some threshold noise level is exceeded, which complicates interpretation.

TRANSMISSION SOURCES A fair evaluation of the effectiveness of different transmission source combinations requires that we compare sources of equal strength. In simulations of different sources we have therefore maintained the total gamma-ray emission rate from the transmission source mixture at a constant value. The reasoning here is that the principle limitation on the count rate for TGS or SGS systems will be the amplifier shaping time, which is independent of the energy distribution of the gamma rays. Moreover, we assume that even though high-energy gamma rays are detected with a lower (full-energy) counting efficiency than low-energy gamma rays, they contribute equally to the count rate limits.

The unattenuated transmission gamma-ray rate $t_{max,p}$ used in the simulations for the p'th peak was computed using

$$t_{max,p} = 10^4 \cdot f_p \cdot f_s \cdot \varepsilon(E_p) ,$$

where f_p is the fractional gamma ray emission of the p'th peak from the s'th source, f_s is the fractional amount of source s (from which gamma ray p is emitted) in the source mixture, and $\varepsilon(E_p)$ is the relative full-energy counting efficiency of the system at the energy E_p of the p'th gamma ray. The efficiency term amounts to a penalty for the use of higher energy gamma rays. Table II lists the values of $t_{max,p}$, f_p, and $\varepsilon(E_p)$ for the transmission sources considered in this study. Figure 1 shows graphically the energies of the different gamma rays, with relative values of $t_{max,p}$ for the pure sources ($f_s = 1$) indicated by the size of the bars. The charts
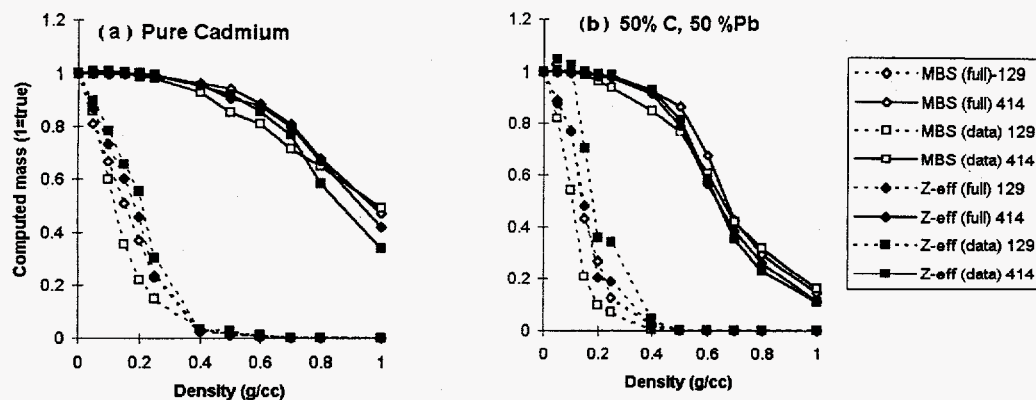
Figure 2. Comparison of simulated 129- and 414-keV TGS assays of ^{239}Pu as a function of matrix density using the MBS (n_z=3) and Z-effective full- and data-coupled attenuation mapping methods. The correct mass in all cases is 1. Note that these results are unrealistically poor compared with actual TGS assays. (a) Assays in a pure cadmium matrix. (b) Assays in a matrix with equal masses of carbon and lead.

for the different isotopes are stacked in order of increasing halflife (highest position equals highest halflife). Generally, the higher the halflife, the better. However, at 1200 years the halflife of ^{166m}Ho is longer than one would like, as its low specific activity means that a source intense enough for transmission imaging must be physically large. This means that a significant Compton background will be added to the spectrum coming out of the source and that the relative intensity distribution will be skewed toward higher energies. No attempt is made here to simulate these effects. The double asterisks on the 265-keV ^{75}Se, 410-keV ^{166m}Ho, and 662-keV ^{137}Cs gamma rays in Table II are reminders that these gamma rays have significant interferences in Pu assays.

RESULTS

COMPARISON OF ATTENUATION MAPPING TECHNIQUES Figure 2a compares the average 129-keV and 414-keV ^{239}Pu masses computed for simulated assays (30 trials for each data point) as a function of the total matrix density using the MBS and the Z-effective methods in both the data-coupled and full coupled schemes. The reader is reminded that accurate 414-keV TGS results are obtained at densities of 1 g/cm³ when using optimal reconstruction algorithms; the poor results here are due to our use of the NNLS algorithm.

The drum matrix is pure cadmium (Z = 48), which is the middle element in the three-element C-Cd-Pb basis set used in our MBS fits. Both the Z-effective and MBS methods are in principle capable of perfect accuracy for this case, although with noisy data the Z-effective method would be expected to give better results. This is because the Z-effective method constrains the matrix to be composed of pure elements (which this matrix happens to be) while the MBS method is free to use mixtures of carbon and lead to improve the fit. The transmission source used was a 1:1:1 (total gamma-ray intensity) mixture of ^{133}Ba, ^{54}Mn, and ^{60}Co. We can see that for this case the Z-effective results are slightly better than those for the MBS method, and that for both cases the results using the full coupling scheme are slightly better than those obtained with the data-coupled scheme. Figure 2b shows the results for the same simulations as in Fig. 2a, this time computed for a 50% C, 50% Pb matrix. In this case only the MBS method is capable of perfect accuracy (C and Pb are the other two basis set elements), while the accuracy of the Z-effective method should be at its worst. We can see, however, that the Z-effective results are only slightly worse than those for the MBS method. In fact, the advantage the MBS method has in describing high/low-Z mixtures appears to be roughly the same as the advantage the Z-effective method has in describing pure elements. The reason for this is that in order for the small inaccuracies in either method to appear as a significant assay bias, the attenuation must
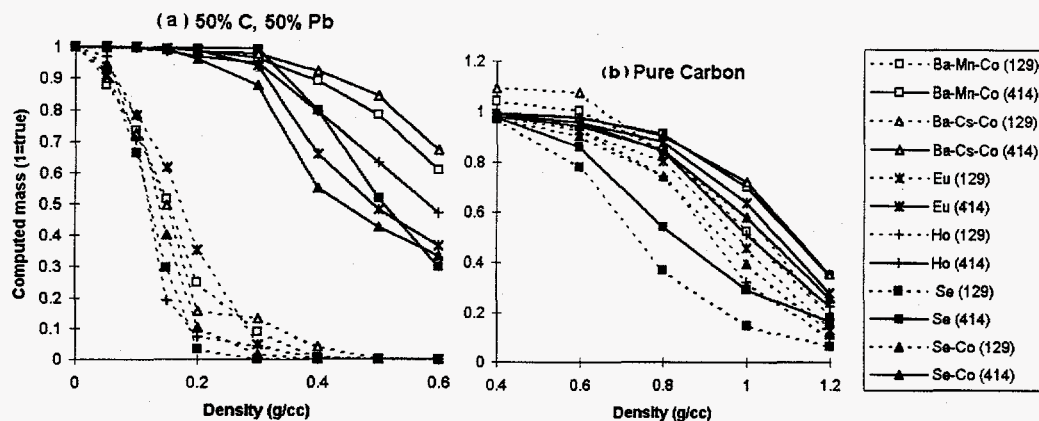
Figure 3. Comparison of simulated 129- and 414-keV TGS assays of ^{239}Pu as a function of matrix density using six different transmission source combinations. The correct mass is 1 in all cases. Note that these results are unrealistically poor compared with actual TGS assays. The isotopes used are ^{133}Ba (Ba), ^{54}Mn (Mn), ^{137}Cs (Cs), ^{152}Eu (Eu), ^{166m}Ho (Ho), ^{60}Co (Co), and ^{75}Se (Se). Ba-Mn-Co and Ba-Cs-Co are 1:1:1 mixtures, while Se-Co is 4:1. (a) Results in a matrix with equal masses of carbon and lead. (b) Results in a pure carbon matrix.

be so large that statistical counting error will overshadow the bias. Similar results are obtained with a low-Z matrix. We conclude that there is no significant advantage in using either the Z-effective or MBS method over the other. Although the fully coupled results are slightly better than the data coupled results,
it is not clear that the difference is large enough to justify the inconvenience and increased computation time of the fully coupled approach.

COMPARISON OF TRANSMISSION SOURCES Figures 3a and 3b summarize the results of our comparison of transmission source combinations for use in TGS systems. All reconstructions were performed using the fully coupled MBS method. The reader is reminded that accurate 414-keV TGS results are obtained at densities of 1 g/cm^3 when using optimal TGS reconstruction algorithms; the poor results here are due to our use of the NNLS algorithm. The source combinations simulated were the pure sources ^{75}Se, ^{152}Eu, and ^{166m}Ho, along with the mixed sources 4:1 ^{75}Se-^{60}Co, 1:1:1 ^{133}Ba-^{54}Mn-^{137}Cs, and 1:1:1 ^{133}Ba-^{137}Cs-^{60}Co. Significant interference lines were excluded, except for the mixture with ^{137}Cs, which was simulated only for illustrative purposes.

Figure 3a shows average 129-keV and 414-keV Pu^{239} assay masses as a function of the matrix density for a sample containing equal partial

densities of carbon and lead. Z-effective for such a matrix is approximately 60 (neodymium). This would approximate a drum containing lead foil or leaded gloves with a low-Z filler such as paper or polyethylene, or a medium-Z matrix such as tantalum crucibles. Figure 3b shows similar results for the same source combinations, but this time for a pure carbon (low-Z) matrix. From the figures, we can subjectively rate the transmission sources in order of effectiveness (most effective first, with the ^{137}Cs mixture omitted), as follows.

Medium Z:
Ba-Mn-Co > Ho ≈ Se > Eu > Se-Co
Low Z:
Ba-Mn-Co > Eu > Se-Co > Ho > Se

Other combinations were tested that are not shown in the figures. In particular, a 1:1 mixture of the inexpensive and long-lived isotopes ^{133}Ba and ^{60}Co (10.5 y and 5.27 y halflives) performed almost identically to the costly ^{166m}Ho, and small added proportions of ^{54}Mn improved the performance significantly. A reasonable low-maintenance source would be a 45% ^{133}Ba, 10% ^{54}Mn, and 45% ^{60}Co mixture. If one neglected to replace the relatively short-lived (313 d) ^{54}Mn, the consequences would not be serious. On the other hand, with diligent maintainance the source would improve over time, as progressively

stronger replacement ^{54}Mn sources could be used to make up for the decay of ^{60}Co and ^{133}Ba.

The observed order of transmission source effectiveness can be understood in terms of nuclear counting statistics. A large number of peaks, as in ^{152}Eu and ^{166m}Ho, reduces the effectiveness of the source by increasing the total amount of background that must be subtracted. It is preferable to have a few, more intense gamma rays. Note that in terms of background contribution, the 1173 and 1332 keV gamma rays in ^{60}Co can probably be considered as one peak. As a rule, when the transmission gamma rays are spread out in energy they will give a better fit to the attenuation function than when they are bunched together. However, transmission gamma rays that are lower in energy than the emission gamma rays they are correcting for will be ineffective when most needed; that is, when the attenuation correction becomes large. In the case of SGS and TGS transmission sources, it appears that extrapolation from higher energy works better than interpolation.

An interesting feature in Fig. 3a is that ^{75}Se gives a very good correction at the density where assays with the other sources first begin to show significant error, but its effectiveness declines steeply at higher densities. The explanation for this is that ^{75}Se was the only source combination considered that has no high-energy gamma rays.

SUMMARY

We found no significant difference in the effectiveness of the four attenuation mapping methods studied here when used with the NNLS and SBS algorithms. For solving large problems, the significantly faster data-coupled methods would therefore be preferred. Results may vary when using different image reconstruction methods, so caution should be exercised when translating the results here to other contexts.

A 1:1:1 (total gamma ray intensity) mixed source of ^{133}Ba, ^{54}Mn, and ^{60}Co appears to perform significantly better than the usual ^{75}Se source for low-burnup Pu assays. Moreover, this single source mixture should effectively replace the entire list of recommended transmission sources in table I for multiple-isotope assays. The shortest-lived nuclide in the mixture, ^{54}Mn, has

2.6 times the halflife of ^{75}Se. The sources ^{152}Eu, ^{166m}Ho, and a 1:1 mixture of ^{133}Ba and ^{60}Co performed at least as well ^{75}Se for ^{239}Pu assays, are all significantly longer lived, and could all be used for multiple-isotope assays.

REFERENCES

1. R. J. Estep, T. H. Prettyman, and G. A. Sheppard, "Tomographic gamma scanning to assay heterogeneous radioactive waste," Nucl. Sci. and Eng. **118**, 145-152.

2. T. H. Prettyman, R. A. Cole, R. J. Estep, and G. A. Sheppard, "A maximum-likelihood reconstruction algorithm for tomographic gamma-ray nondestructive assay," Nucl. Inst. and Meth. **A356**, 470-475.

3. J. L. Parker in "Passive nondestructive assay of nuclear materials," chapters 4-6. D. Reilly, et al. editor. Nucl. Reg. Comm. document NUREG/CR-5550 (1991).

4. Martz, et al., "Quantitative waste assay using gamma-ray spectrometry and computed tomography," Proc. 14th Annual Mtg., Salamanca, Spain, May 5-8, 1992, European Safeguards Research and Development Association (1992).

5. T. H. Prettyman, et al. To be published.

6. R. J. Estep, T. H. Prettyman, and G. A. Sheppard, "Reduction of TGS image reconstruction times using separable attenuation coefficient models," ANS Winter Meeting Transactions, Fall 1995, San Francisco, CA.

7. R. J. Estep, "TGS_FIT 3.0: Image reconstruction software for quantitative, low-resolution tomographic assays," to be published, Los Alamos National Laboratory.

8. R. J. Estep, "TGS_FIT: Image reconstruction software for quantitative, low-resolution tomographic assays," LA-12497-MS, Los Alamos National Laboratory (1993).